Interlayer structure and dynamics of Cl-bearing hydrotalcite: far infrared spectroscopy and molecular dynamics modeling

JIANWEI WANG,[1,*] ANDREY G. KALINICHEV,[1] JAMES E. AMONETTE,[2] AND R. JAMES KIRKPATRICK[1]

[1]Department of Geology, University of Illinois at Urbana-Champaign, 1301 W. Green St., Urbana, Illinois 61801, U.S.A.
[2]Environmental Molecular Sciences Laboratory, Pacific Northwest National Laboratory, P.O. Box 999, K8-96, Richland, Washington 99352, U.S.A.

ABSTRACT

Comparison of the observed far-infrared (FIR) spectrum of Cl^--containing hydrotalcite, $[Mg_3Al(OH)_8]Cl \cdot 3H_2O$, to a power spectrum calculated using molecular dynamics (MD) computer simulation, provides a greatly increased understanding of the structure and vibrational dynamics in the interlayers of layered double hydroxides. Good agreement between the observed FIR band positions and the simulated power spectrum illustrates the capability of this combination of experimental and computational techniques to effectively probe the structure and dynamics of water in nano-pores and other confined spaces. The simulation model assumes an ordered Mg_3Al arrangement in the octahedral sheet and no constraints on the movement of any atoms or on the geometry and symmetry of the simulation supercell. Calculated anisotropic components of the individual atomic power spectra in combination with computed animations of the vibrational modes from normal mode analysis allow for reliable interpretations of the observed spectral bands. For the vibrations related to octahedral cation motions, bands near 145, 180, and 250 cm^{-1} are due dominantly to Mg vibration in the **c** direction (perpendicular to the hydroxide layers), Al vibration in the **c** direction, and Mg and Al vibrations in the **a-b** plane (parallel to the hydroxide layers), respectively. The low frequency vibrational motions of the interlayer are controlled by a network of hydrogen bonds formed between interlayer water molecules, Cl^- ions, and the OH groups of the main hydroxide layers. The bands near 40–70 cm^{-1} are related to the translational motions of interlayer Cl^- and H_2O in the **a-b** plane, and the bands near 120 cm^{-1} and 210 cm^{-1} are largely due to translational motions of the interlayer species in the **c** direction. The three librational modes of interlayer water molecules near 390, 450, and 540 cm^{-1} correspond to twisting, rocking, and wagging hindered rotations, respectively. The spectral components of the interlayer Cl^- motions are remarkably similar to those of bulk aqueous chloride solutions, reflecting the structural and dynamic similarity of the nearest-neighbor Cl^- environments in the interlayer and in solution.

INTRODUCTION

The structural arrangement and dynamical behavior of H_2O molecules, ions, and other molecular species in the confined spaces of nano-scale pores and mineral interlayers are key to understanding transport and reactivity in many geochemical, technological, and biological systems. In recent years there have been significant experimental and computational efforts to understand the structure and dynamics of aqueous species in heterogeneous systems (e.g., Nandi et al. 2000; Dore 2000), including clays and other layered minerals (Kagunya 1996; Kagunya et al. 1997; Smirnov and Bougeard 1999; Greathouse et al. 2000; Swenson et al. 2000). Most of these experimental and computational studies focused on the effects of confinement on the structure and dynamics of H_2O molecules relative to the properties of bulk liquid water. Here we present a combined experimental far-infrared spectroscopic (FIR) and computational molecular modeling study of the Cl^--containing

layered double hydroxide (LDH) compound hydrotalcite, $[Mg_3Al(OH)_8]Cl \cdot 3H_2O$. These results complement the results of our previous NMR and molecular dynamics (MD) modeling studies of LDH phases (Kirkpatrick et al. 1999; Hou et al. 2000, 2002; Kalinichev et al. 2000; Hou and Kirkpatrick 2000, 2002; Wang et al. 2001; Kalinichev and Kirkpatrick 2002), demonstrate the capabilities of this combined approach to greatly improve our understanding and interpretation of the relatively low frequency vibrational dynamics of ions and water molecules in confined fluids, and provide significant new insights into the structure and dynamics of LDH phases.

LDHs are unusual among oxide and hydroxide materials in having large permanent positive layer charges and, consequently, large anion exchange capacities. Interest in these phases, which are also known as hydrotalcite-like compounds (HTs), mixed-metal layered hydroxides (MMLHs), and anionic clays, has increased rapidly in recent years. This interest is due to their role in a wide range of natural and hazardous waste environments, in Portland cements, their use as catalysts, catalyst supports, carriers for drugs, electrode modifiers, and in

---

* E-mail: jwang7@uiuc.edu

other technological applications (e.g., Cavani et al. 1991; Newman and Jones 1998; Basile et al. 2001). LDHs can be synthesized with a wide range of main (hydroxide) layer cations and interlayer organic and inorganic anions (Miyata 1975, 1983; Newman and Jones 1998; Costantino et al. 1998). These materials thus offer an excellent opportunity to investigate fundamental structural and dynamical properties of interlayer and surface species and are important models for understanding aqueous solutions confined in nano-pores (Kagunya 1996; Kagunya et al. 1997; Kirkpatrick et al. 1999; Kalinichev et al. 2000; Hou and Kirkpatrick 2000, 2002; Hou et al. 2000, 2002; Wang et al. 2001; Kalinichev and Kirkpatrick 2002). The positive layer charge of LDHs contrasts with the negative layer charges typical of aluminosilicate clays.

The structures of most LDHs consist of single-layer metal hydroxide sheets alternating with interlayers that contain anions and water molecules (e.g., Taylor 1973; Bellotto et al. 1996; Newman and Jones 1998). The hydroxide sheets develop positive charge through cation substitution, which is compensated for by the interlayer and surface anions. In many LDHs, including the phase studied here, the hydroxide layer can be thought of as a trioctahedral, brucite-type sheet of composition $[M^{2+}(OH)_2]$ in which some of the 2+ cations are replaced by higher charge cations. A typical structural formula is $(M_{1-x}^{2+}M_x^{3+})(OH)_2 \cdot A_{x/n}^{-n} \cdot mH_2O$, where x is the fraction of 3+ cations in the structure, n is the anionic charge, and m is the number of water molecules per formula unit.

Vibrational spectroscopy has played an important role in understanding the structures of LDHs (Hernandez-Moreno et al. 1985; Kagunya et al. 1998; Frost et al. 2000; Kloprogge et al. 2001). However, the focus has been principally on the higher-frequency bands in the mid-infrared range (4000–400 cm^{-1}) associated with vibrations of the octahedral sheets and the interlayer species.

Kagunya et al. (1998) studied several Mg/Al hydrotalcite compounds, although not the Cl$^-$ phase. Their IR, Raman, and inelastic neutron scattering (INS) data and their vibrational mode analysis provide an important basis for the interpretations given here. Kagunya et al. (1998) assumed that the octahedral sites of the hydroxide layer have D_{3d} symmetry, that there is complete cation disorder over the octahedral sites, and that there is only a single cation position. Thus, their vibrational band assignments were based on those for simple hydroxides such as Mg(OH)$_2$. However, Al^{3+} and Mg^{2+} have quite different charge to radius ratios (z/r), and there is substantial evidence for strong short-range Mg/Al ordering at the octahedral sites in Mg/Al LDHs (Vucelic et al. 1997; Cai et al. 1994; Yao et al. 1998). Additionally, the network of hydrogen bonds among the interlayer water molecules and anions and main layer OH-groups is known to be structurally and dynamically disordered (Kirkpatrick et al. 1999; Wang et al. 2001). The simplifying assumptions of Kagunya et al. (1998) limited their ability to effectively assign and analyze the vibrational bands in the FIR region below 400 cm^{-1}.

The FIR spectra of LDHs reflect the low-frequency lattice vibrations associated with torsional motions of the hydroxide octahedra (e.g., Ruan et al. 2002), as well as intermolecular vibrations resulting from the complex combination of relatively weak hydrogen-bonding interactions within the anion-water interlayers and between these interlayers and main hydroxide layers. These low-frequency vibrational modes are especially important for characterization of LDH phases, because they are most sensitive to the changes of the interlayer structure and dynamics. The intermolecular modes involve the relative motions of interlayer species as a whole and may be of either translational or librational (rotational) origin. The translational vibrations depend upon the total molecular mass, whereas the rotational vibrations are functions of molecular moments of inertia and are expected to have higher intensity in the spectra (Finch et al. 1970).

The MD simulations reported here use the newly developed CLAYFF force field (Cygan et al., manuscript in preparation), which has already proven highly efficient in modeling the structures of many oxide, hydroxide, and clay phases, the interaction of aqueous solutions and their dissolved species with mineral surfaces, and the behavior of interlayer ions and water (Cygan 2001; Kalinichev et al. 2000; Wang et al. 2001; Hou et al. 2002; Kalinichev and Kirkpatrick 2002). Although the force field was not specifically optimized to simulate either LDHs or vibrational frequencies, the computed power spectra of the low frequency atomic motions described here are in good agreement with the observed FIR spectrum, and the results allow for reliable interpretation of the observed vibrational bands.

METHODS

Structural model

The model structure was based on the crystal structure of Mg/Al hydrotalcite determined by Bellotto et al. (1996) from powder X-ray diffraction data using Rietveld methods. This structure is broadly similar to that of hydrocalumite, for which the structure has been refined from single-crystal X-ray diffraction data (Terzis et al. 1987). However, the structure of hydrotalcite is not as well constrained because it is based on powder X-ray data. The Mg/Al hydrotalcite structure has previously been refined in a rhombohedral unit cell with the space group $R\bar{3}m$ (Bellotto et al. 1996, Vucelic et al. 1997). Thus, rhombohedral $R\bar{3}m$ symmetry was used for the initial hydroxide layer configuration, but the simulation supercell was converted to $P1$ symmetry before starting the simulations, and no further constraints were imposed on the cell parameters or symmetry. In our model, the Mg/Al ratio was set to 3. Long-range cation ordering in LDHs has been difficult to observe by powder X-ray diffraction, except for the Ca/Al, Li/Al, and Mg/Ga phases (Bellotto et al. 1996; Terzis et al. 1987). However, evidence for significant short-range cation ordering in other LDHs comes from X-ray absorption spectroscopy and nanoscale imaging of molecular sorption onto crystal surfaces (Vucelic et al. 1997; Cai et al. 1994; Yao et al. 1998). XAS shows the absence of Fe-Fe neighbors in Mg/Fe hydrotalcite, suggesting domains of cation ordering with dimensions on the order of a few nanometers (Vucelic et al. 1997). Similar short-range ordering is expected in Mg/Al hydrotalcite. In support of this conclusion, AFM and STM images show ordered two-dimensional lattices of organic and inorganic anions adsorbed on the (001) surfaces of Mg/Al hydrotalcite crystals (Cai et al. 1994;

Yao et al. 1998). Thus, in our models, complete Mg/Al ordering was assumed, and each $Al(OH)_6$ octahedron had six nearest-neighbor $Mg(OH)_6$ polyhedra.

The periodic supercell for MD simulations consisted of 36 crystallographic unit cells, $6 \times 6 \times 1$ in the **a**-, **b**-, and **c**-directions respectively. Thus, the model contained three octahedral sheets, each with 27 Mg and 9 Al, and three interlayers, with 9 Cl^- and 27 H_2O each. Chloride ions and water molecules were initially randomly distributed in the interlayer space to give a total composition of $[Mg_3Al(OH)_8]Cl\cdot3H_2O$.

MD simulations

Computational molecular modeling is based on the use of interatomic potentials (e.g., a force field) that effectively and accurately account for the interactions of all atoms in the modeled system (e.g., Cygan et al. 2001). The dynamics of solid substances can be explicitly modeled by introducing a set of bonded interaction terms based on experimental X-ray diffraction structural data and quantum chemical calculations (e.g., Hill and Sauer 1994, 1995; Teppen et al. 1997; Bougeard et al. 2000). In this approach, all bonds in the structure must be initially identified and evaluated for each possible interatomic coordination. However, application of such an approach to systems with complex and ill-defined bond structures (such as clays and LDHs) is often problematic, because it can lead to significant over-parameterization of the force field, due to lack of the experimental data to constrain all the parameters necessary to explicitly describe bonded interactions.

The CLAYFF force field used in our simulations is based on an alternative approach to the description of the metal-O atom interactions in hydrated phases that incorporates these interactions as ionic (i.e., non-bonded), thus allowing the simulations of even complex disordered systems. The specific methods and algorithms used for the development and validation of the force field are discussed in detail elsewhere (Cygan et al., manuscript in preparation). Here we mention only that the parameters of the CLAYFF force field are specifically optimized based on the observed structures of simple well-characterized oxides, hydroxides, and oxyhydroxides, with partial atomic charges derived from periodic DFT quantum calculations of these model compounds. The charges on O atoms and H atoms are allowed to vary with nearest-neighbor cation substitution and their occurrence in water molecules, hydroxyl groups, and bridging sites. The potential energy of the model system is calculated as the sum of all atom-atom Coulomb and non-Coulomb (van der Waals) contributions. The non-Coulomb interactions were described by the conventional Lennard-Jones (12–6) function, and the parameters of unlike interactions are calculated according to the arithmetic mean rule for the distance parameter, R_0, and the geometric mean rule for the energetic parameter, D_0. Specific energy expressions and the force field parameters used in this work are listed in Table 1. For water, the flexible version of the simple point charge (SPC) interaction potential was used (Berendsen et al. 1981; Teleman et al. 1987). For consistency with the SPC water model, the van der Waals terms centered on O atoms were assumed equivalent for both H_2O molecules and OH groups of the hydroxide layers, and no individual van der Waals parameters were assigned

TABLE 1. Potential energy expressions and force field parameters used for the MD simulations of $[Mg_3Al(OH)_8]Cl\cdot3H_2O$ in this study

	$D_{0,i}$ (kcal/mol)	$R_{0,i}$ (Å)	q_i (e)
Hydroxide layer			
Mg	9.03E-07	5.91	1.36
Al	1.33E-06	4.79	1.5752
O (hydroxide)	0.1554	3.55	−1.0069
H (hydroxide)	–	–	0.425
Interlayer			
Cl	0.1	4.94	−1.0
O (water)	0.1554	3.55	−0.82
H (water)	–	–	0.41

Note: $E_{\text{Coulomb}} = \dfrac{q_i q_j}{4\pi\varepsilon_0 r_{ij}}$, $E_{vdW} = D_{0,ij}\left[\left(\dfrac{R_{0,ij}}{r_{ij}}\right)^{12} - 2\left(\dfrac{R_{0,ij}}{r_{ij}}\right)^6\right]$,

$R_{0,ij} = (R_{0,i} + R_{0,j})/2$, $D_{0,ij} = \sqrt{D_{0,i}D_{0,j}}$.

to the hydrogen atoms. The force field parameters for aqueous Cl^- were taken from the literature (Smith and Dang 1994).

The MD simulations were performed using periodic boundary conditions, Ewald summation to calculate long-range electrostatic contributions to the potential energy, and a "spline cutoff" method to calculate short-range van der Waals interactions (Molecular Simulations 1999). Two stages of energy minimization were applied to the initial model. First, we fixed the positions of atoms in the octahedral sheets and allowed only the interlayer species to relax, since their initial positions and orientations are most likely to be significantly different from the optimum configurations. Energy minimization was then applied to the entire system with no constraints. The energy of the model system was allowed to converge to its minimum within a 0.001 kcal/mole convergence criterion, and this optimized structure was then used as the starting configuration for *NPT*-ensemble MD simulation at 300 K and 1 bar with a time step of 1.0 fs. The system was allowed to relax and equilibrate for 100 ps of MD simulation. To ensure thermodynamic equilibrium, the convergence of total energy and its components, as well temperature, density, and atomic radial distribution functions were carefully monitored during this equilibration period. The equilibrium dynamic trajectory was finally recorded during the next 40 ps of MD simulation at 8 fs intervals for statistical analysis of the structural and dynamic characteristics of the system. This time resolution is sufficient to reliably calculate the atomic velocity autocorrelation functions (VACFs) and the corresponding power spectra in the FIR range.

Analysis of atomic vibrational dynamics from MD simulations

The computed power spectra were obtained as Fourier transformations of the corresponding VACFs, which were calculated from the MD-simulated dynamic trajectories of atoms in the model system (e.g., McQuarrie 1976; Kleinhesselink and Wolfsberg 1992). The VACFs were calculated for each atomic type as:

$$\text{VACF} \equiv \langle \mathbf{v}(0)\cdot\mathbf{v}(t)\rangle = \frac{1}{N_\tau N}\sum_{i=1}^{N_\tau}\sum_{j=1}^{N}\mathbf{v}_j(t_i)\cdot\mathbf{v}_j(t_i+t) \quad (1)$$

where N_τ is the number of time averages, N is the number of atoms, and $\mathbf{v}_j(t)$ the velocity of atom j at time t. The total VACF

was calculated over all atoms in the system, and atomic VACFs were averaged over all atoms of a given type.

Three anisotropic contributions to the VACFs, *XX*, *YY*, and *ZZ*, were also calculated for each atom type in the same manner but using only the relevant **a**-, **b**-, and **c**-projections of the velocity vectors. Due to the geometry of the simulated system, the **a**- and **b**-components of the atomic velocities are parallel to the metal hydroxide layers, and the **c**-components are perpendicular to the layers. Thus, the *XX* and *YY* VACFs reflect the correlations of atomic motions within the plane parallel to the hydroxide layers and the *ZZ* VACFs reflect those perpendicular to the layers. Power spectra were then calculated for the entire simulation model and separately for each atom type. Decomposition of the calculated power spectra into their anisotropic components due to the atomic motions along different crystallographic directions greatly enhances vibrational band assignment and spectral interpretation. In the model system, most VACFs decay to zero within several picoseconds, providing spectral resolution of about 5–8 cm^{-1} in the FIR frequency range. The power spectra for light atoms such as hydrogen have lower absolute resolution than the other atoms.

Normal mode analysis

Calculation of the normal modes of vibration for the simulated system is a useful aid in visualizing and qualitatively analyzing the complex modes of atomic motions in phases such as LDHs. For a system with *P*1 symmetry, a normal mode analysis yields (3*N*-6) vibrational modes. To speed up calculation of the normal modes without losing significant information, we used a smaller model with 90 atoms and $2 \times 2 \times 1$ crystallographic unit cells in the **a**-, **b**-, and **c**-directions respectively, rather than the 810-atom model used for the MD simulations. The standard calculation (e.g., McMillan and Hess 1988; Kubicki 2001) approximates the potential energy surface as a Taylor series truncated after the second term, and thus only harmonic frequencies can be determined. In addition to this limitation, the series of individual energy-minimized configurations used in the calculation of normal vibrational modes does not completely represent the phase space of a dynamic system at a finite temperature. Thus, such calculations typically yield frequencies and intensities that are somewhat different than those obtained from the power spectrum calculations. Here we used this method only as a visualization and interpretation aid.

Experimental infrared spectra

Far-infrared spectra of a sample compositionally similar to the one used in the MD simulations were collected in transmission mode with Bruker IFS 66v/S and IFS 66/S spectrometers using standard FT-IR techniques. Excellent spectra could be obtained by pressing small amounts of powder onto one side of a piece of Scotch tape. The two spectra reported here (Figs. 1 and 2) were collected with different beam splitters that allow for greater sensitivity in different frequency ranges. Spectrum EXP-1 was collected with the IFS 66v/S instrument under vacuum conditions with a 23 μm Mylar beam splitter, which is nearly opaque around 150 cm^{-1} but is relatively sensitive at other frequencies between 25 and 600 cm^{-1}. Spectrum EXP-2 was collected with the IFS 66/S instrument under N$_2$ purge con-
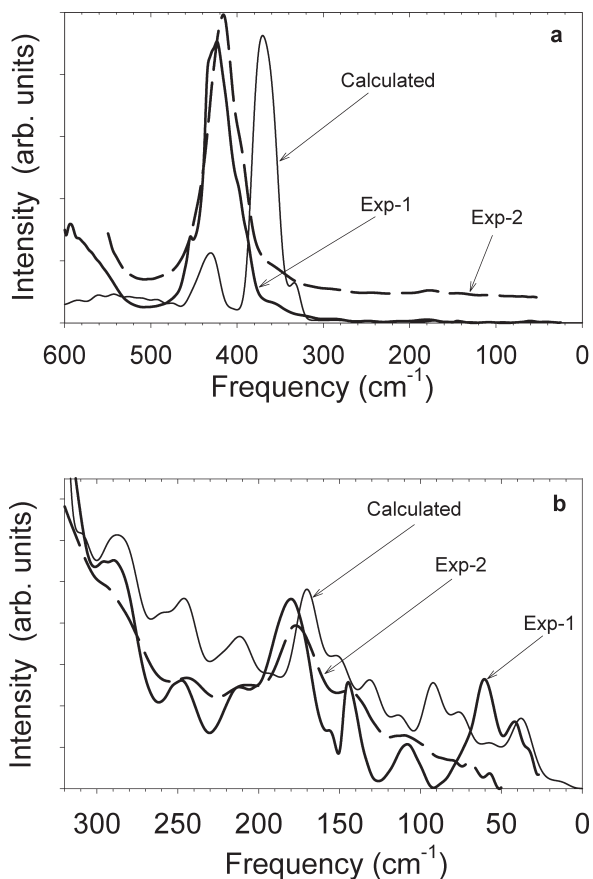
FIGURE 1. (**a**) Measured far-infrared spectra (thick lines) of Mg/Al Cl-bearing hydrotalcite and the calculated power spectrum from MD simulations (thin line). (**b**) Low-frequency region of the same spectra at expanded scale. The intensities of the calculated and measured spectra are scaled for comparison. Exp-1 and Exp-2 are observed spectra of the same sample obtained using two different spectrometers.

ditions with a 6 μm Mylar beam splitter, for which sensitivity is optimal at 150 cm^{-1} and higher frequencies. The band positions in the two spectra are in excellent agreement.

The sample of Cl-bearing hydrotalcite (HT) used in these measurements was synthesized by mixing 0.75 mol/L MgCl$_2$ and 0.25 mol/L AlCl$_3$ solutions at 70 °C, via the co-precipitation method of Miyata (1975) (Hou et al. 2000). The suspension was aged at 70 °C for about 8 h. The solid sample was separated from the solution and recrystallized at 200 °C for 10 days in a Parr vessel under autoclave conditions. The recrystallized solid was then centrifugally separated from the solution, washed and vacuum filtered to remove salts, and dried at 70 °C for 24 h. Powder XRD using a Scintag diffractometer and Cu*K*α radiation showed that the sample was phase-pure. The chemical composition was determined using wet chemical analysis (Kirkpatrick et al. 1999; Hou et al. 2000), and the resulting structural formula was $[Mg_{0.764}Al_{0.236}(OH)_2]$ $(CO_3)_{0.007}Cl_{0.221}\cdot0.7H_2O$. The Mg/Al ratio of about 3.2 is in the normal range for hydrotalcites. The small amount of CO$_3$ is probably from exposure to the atmosphere during and after synthesis and is
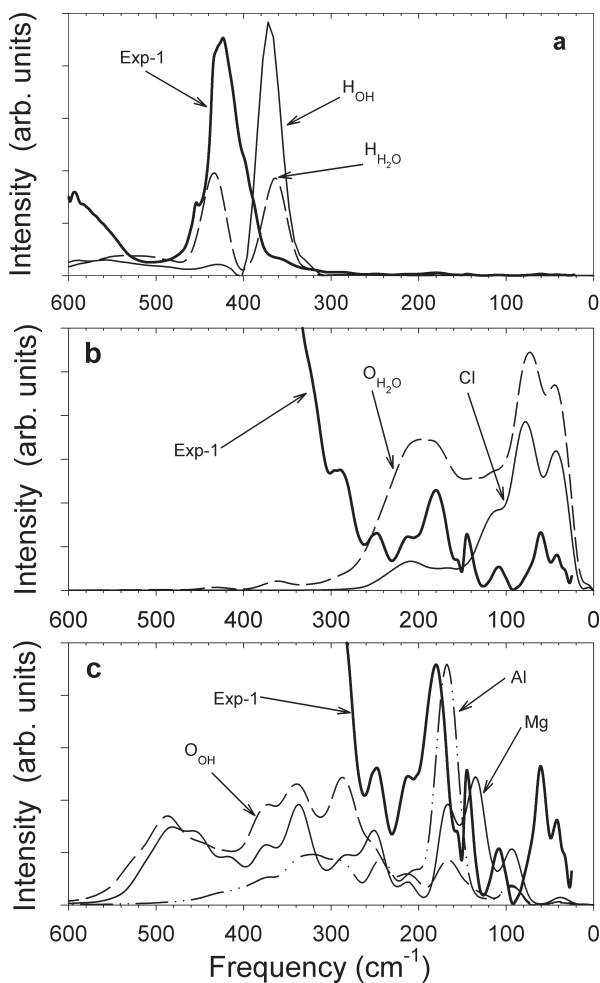
FIGURE 2. Individual atomic contributions to the total calculated power spectrum of Mg/Al Cl-bearing hydrotalcite. Measured FIR spectra are shown for comparison. (**a**) Contributions due to the proton dynamics of OH groups and water molecules. (**b**) Molecular contributions of interlayer species (Cl⁻ and H₂O). (**c**) Contributions due to the lattice dynamics of the Mg/Al octahedral hydroxide layers. H_{OH}, H_{H2O}, O_{OH}, and O_{H2O} stand for hydrogen atoms of OH groups, hydrogen atoms of water molecules, O atoms of OH groups, and O atoms of water molecules.

in the range normally observed. The amount of water is also in the normal range and close to the standard formula.

RESULTS AND DISCUSSION

Comparison of observed and MD simulated spectra

The similarity between the band frequencies in the computed power spectra and observed FIR spectra are expected to be limited principally by the quality of the force field used in the simulations. The results reported here are surprisingly good given that the CLAYFF force field is not optimized for either vibrational frequencies or the structures of LDH compounds, contains only electrostatic and van der Waals terms, and apart from the intramolecular harmonic stretching and bending terms for H₂O molecules and OH groups, contains no parameters

explicitly related to the interatomic bonding and vibrations. Experimental IR band intensities are related to fluctuations of the dipole moment due to atomic and molecular vibrations (McMillan and Hess 1988; Kagunya et al. 1998; Bougeard et al. 2000), whereas the intensity in the total computed power spectrum includes contributions from all atomic motions recorded in the VACF. However, each moving atom in the simulation model bears a charge, and all atomic motions result in fluctuations of the system's dipole moment. Thus, the two phenomena are strongly related. The calculated and experimental band intensities, however, cannot be directly compared. The analysis here focuses largely on the band positions.

The observed FIR spectra contain several strong bands in the range from 350 to 475 cm⁻¹ (Fig. 1a, Table 2) and weaker but well resolved bands in the lower frequency range from 25 to 350 cm⁻¹ (Fig. 1b, Table 2). The computed power spectrum contains three major bands in the range from 325 to 450 cm⁻¹, in good qualitative agreement with the observed spectrum (Fig. 1a, Table 2). The frequencies of these calculated bands are about 20–50 cm⁻¹ lower than the observed frequencies. In the lower frequency range (Fig. 1b), there is even better correspondence between the frequencies in the measured and calculated spectra. For most bands, the observed and computed frequencies are nearly the same, but those at 145, 157, and 180 cm⁻¹ in the observed spectrum are shifted about 4–13 cm⁻¹ to 132, 153, and 171 cm⁻¹ in the calculated spectrum.

The power spectra for individual atom types are key to making band assignments and interpretations (Figs. 2a–c). The power spectra for the hydrogen atoms of water molecules and OH-groups of the hydroxyl layer show that the bands in the 350 to 475 cm⁻¹ range are due to motions involving these species (Fig. 2a). The modes related to the hydrogen atoms of the main layer OH groups occur at 370 cm⁻¹ in the computed spectrum, and those of hydrogen atoms in interlayer water molecules occur in three bands at about 360, 430, and 540 cm⁻¹. At lower frequencies between 40–240 cm⁻¹ the bands due to interlayer Cl⁻ and the O atoms of interlayer water are very similar (Fig. 2b). Both species contribute to groups of bands from 40 to 120 cm⁻¹ and near 210 cm⁻¹. Likewise, the spectral contributions due to the Mg, Al, and O of OH motions are also strongly correlated (Fig. 2c). All have bands near 90, 170, and 330 cm⁻¹. Al and Mg have a band near 250 cm⁻¹, and Mg and O have a band near 480 cm⁻¹. Mg has a strong band near 130 cm⁻¹, and the O atom of hydroxyl groups have a band near 290 cm⁻¹.

The computed anisotropic *XX*, *YY*, and *ZZ* components of the individual atom power spectra allow for even more specific band interpretations (Figs. 3, 4, 5 and Table 2). For LDHs, the *XX* and *YY* components for a given atom type are nearly identical, and therefore the *YY* components are not shown in Figures 3–5. The *ZZ* component is substantially different, as expected for a structure with layering perpendicular to the **c**-direction. For the O atoms in interlayer water molecules (Fig. 3a), the bands from 40 to 85 cm⁻¹ are due mainly to the *XX/YY* components, and the band near 210 cm⁻¹ is mainly to the *ZZ* component. For interlayer Cl⁻ atoms (Fig. 3b), the band near 120 cm⁻¹ is due principally to the *ZZ* component and the bands near 40 and 210 cm⁻¹ to the *XX/YY* components. The Cl⁻ band

TABLE 2. Measured and calculated spectral bands of $Mg_3Al(OH)_8 \cdot Cl \cdot 3H_2O$ hydrotalcite in the far-infrared range of frequencies

Experimental cm⁻¹	Calculated cm⁻¹	Notes
33 vw 42 w	38 m	40 cm⁻¹ band, Cl and some H_2O translations in the **a-b** plane (hydrogen bond bending)
60 w	58 w	60 cm⁻¹ band, H_2O translations in the **a-b** plane (hydrogen bond bending)
78 vw	76 w	80 cm⁻¹ band, Cl translations in all directions and some H_2O translations in **a-b** plane
87 vw	92 s	90 cm⁻¹ band, Mg in **c** (A_{2u}) overlapped with the Al and OH motions in the **a-b** plane (E_u)
109 w	114 w	120 cm⁻¹ band, Cl **c** translations
145 w	132 m	130 cm⁻¹ band, Mg translational vibrations along **c** (A_{2u})
157 w	153 w	150 cm⁻¹ band, OH motions in the **a-b** plane ($E_u + E_g$)
180 w	171 s	170 cm⁻¹ band, Al vibrations along **c** (A_{2u}), overlapped with OH motions in the **a-b** plane ($E_u + E_g$)
213 vw	212 m	210 cm⁻¹ band, H_2O translations along **c** (hydrogen bond stretching) and Cl in **a-b** plane
248 v 254 vw	247 m 260 w	250 cm⁻¹ band, Mg and Al vibrations in the **a-b** plane (E_u)
290 w	288 m	290 cm⁻¹ band, O of OH motions in the in **a-b** plane ($E_g + E_u$)
296 w	310 w	310 cm⁻¹ band, H of OH in **a-b** and **c** motions
359 m	334 m	330 cm⁻¹ band, H of H_2O in **a-b**, H of OH in **c** motions; overlaps with translational vibrations of Mg ($A_{2u} + E_g$), Al (E_u), and O in the distorted hydroxide octahedra
388 s 399 s	361 w	360 cm⁻¹ band, H_2O twisting librations (hindered rotations)
424 vs 434 vs	371 vs 406 w	370 cm⁻¹ band, OH motions along **c** (A_{1g})
454 s	430 vs	430 cm⁻¹ band, H_2O rocking librations (hindered rotations) 480 cm⁻¹ band, Mg in the **a-b** plane (E_u), and OH along **c** (A_{1g}) 540 cm⁻¹ band, H_2O wagging librations (hindered rotations)

Notes: Band notations: vw = very weak; w = weak; m = medium; s = strong; vs = very strong

near 80 cm⁻¹ has contributions from all of the three components. For the hydrogen atoms of interlayer water molecules (Fig. 4a), the two bands near 370 and 430 cm⁻¹ are due principally to the *XX/YY* components, and the band near 540 cm⁻¹ is dominated by the *ZZ* component. For the hydrogen atoms of OH molecules (Fig. 4b), the major band near 370 cm⁻¹ and the two shoulders at 360 and 430 cm⁻¹ are due principally to the *ZZ* component, whereas the broad band near 580 cm⁻¹ is due mainly to the *XX/YY* components. For Mg atoms of the octahedral sheet (Fig. 5a), the bands near 90 and 130 cm⁻¹ are due to the motions contributing to the *ZZ* component, those near 250 and 480 cm⁻¹ mainly to the *XX/YY* components, and those near 330 and 170 cm⁻¹ to all three. Similarly, for octahedrally coordinated Al (Fig. 5b), the band near 170 cm⁻¹ is due mainly to the *ZZ* component and those near 90, 250, and 330 cm⁻¹ are due mainly to the *XX/YY* components. For the O atoms of OH groups (Fig. 5c), the bands near 480 and 370 cm⁻¹ are associated with the motions contributing mainly to the *ZZ* component, and the bands near 330, 290, and 170 cm⁻¹ are due mainly to the *XX/YY* components.

FIGURE 3. Anisotropic contributions to the power spectra of interlayer species: (**a**) O of H_2O; (**b**) Cl⁻. Solid lines are total atomic power spectra; dashed lines are *ZZ* spectral components due to atomic motions in the **c** direction (perpendicular to the layers); dash-dot lines are *XX* and *YY* spectral components due to atomic motions in the **a-b** plane (parallel to the layers). ▶
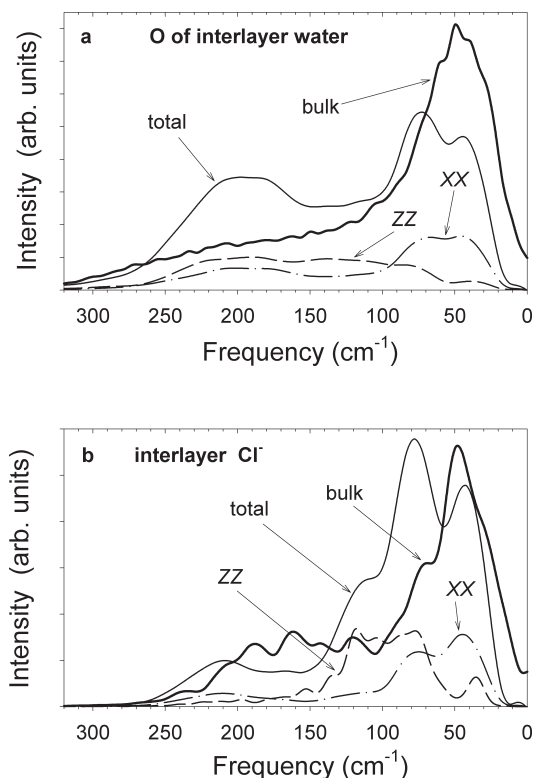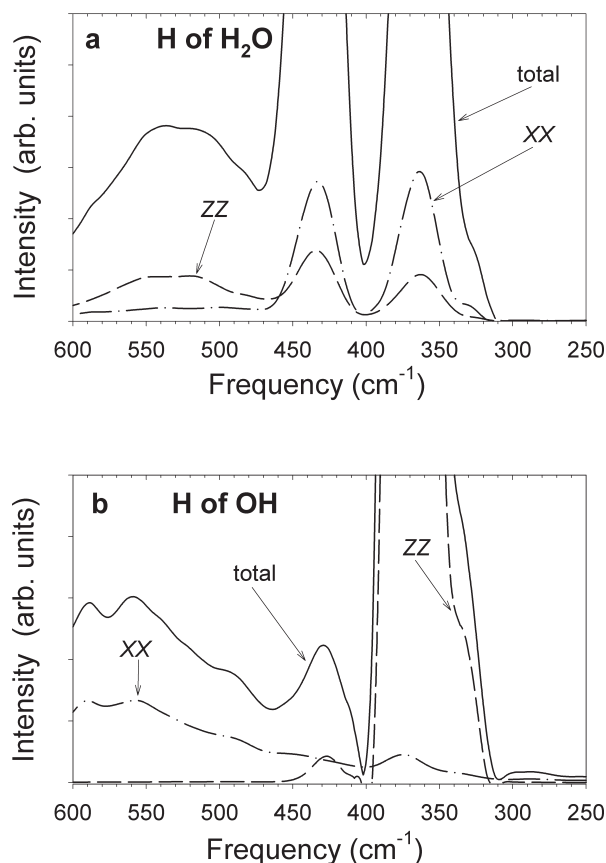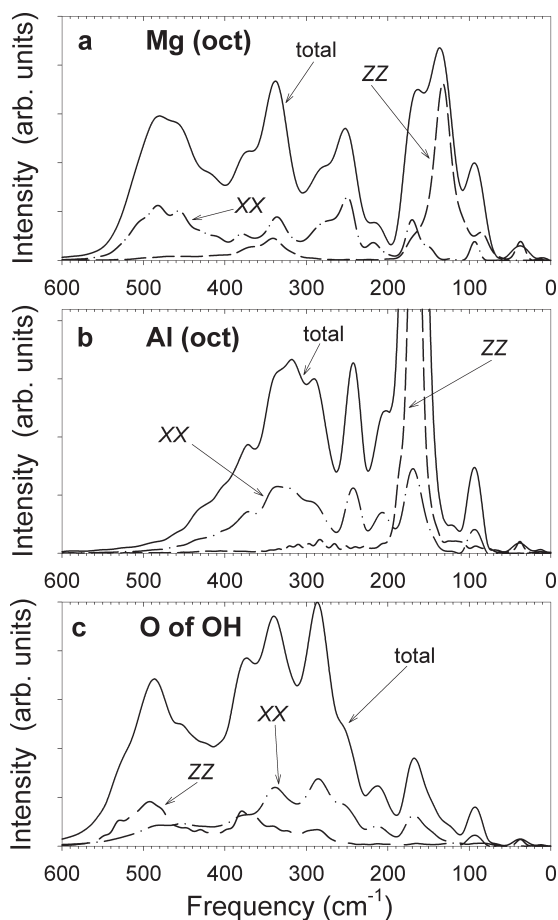
FIGURE 4. Anisotropic contributions to the power spectra of protons in the librational range of frequencies: (**a**) H of interlayer H_2O molecules; (**b**) H of hydroxyl groups in the main octahedral sheets. *XX, YY,* and *ZZ* notations of individual components are as in Figure 3.

FIGURE 5. Anisotropic contributions to the lattice dynamics of Mg/Al octahedral hydroxide layers: (**a**) Mg of the hydroxide layers; (**b**) Al of the hydroxide layers; (**c**) O of the hydroxide layers. *XX, YY,* and *ZZ* notations of individual components are as in Figure 3.

The computed normal modes of vibrations also provide important insight into band interpretation. These modes form several groups corresponding to the vibrational bands in the power spectra. For instance, the modes in the 40 to 100 cm^{-1} range are due to the interlayer species undergoing translational motions in the **a-b** plane with the octahedral sheets essentially stationary. This is in good agreement with the individual atom and anisotropic power spectra calculated from MD simulations. The normal modes in the range from 118 to 130 cm^{-1} and from 215 to 235 cm^{-1} are mainly due to the translational vibrations of interlayer species perpendicular to the layers. The normal modes between 150 and 165 cm^{-1} are associated with Mg translational motions in the **c**-direction, which occurs near 130 cm^{-1} in the power spectrum computed from the MD trajectory. Likewise, the normal modes in the range between 189 and 196 cm^{-1} are due to the translational motions of Al in the **c**-direction, which occurs near 170 cm^{-1} in the MD-simulated power spectrum. The normal modes in the range between 245 and 260 cm^{-1} are associated with Mg and Al translational motions in the **a-b** plane, which occur near 250 cm^{-1} in the MD-simulated power spectrum.

Table 2 lists our band interpretations and assignments for the computed and observed spectra, and we now discuss these assignments and related atomic motions in more detail.

Crystal structure, atomic motions, and vibrational band assignments

Due to the Mg/Al ordering assumed for our calculations and the distortion of the Mg coordination polyhedron from octahedral symmetry (Wang et al. 2001), the low frequency vibrational modes for the hydroxide layers in our MD simulations are expected to be more complicated than those of the single-metal hydroxide model used by Kagunya et al. (1998). Experimental and computational results for the Cl-containing Mg/Al phase also indicate that the positions of interlayer Cl$^-$ ions and water molecules are disordered (Bellotto et al. 1996; Kirkpatrick et al. 1999; Wang et al. 2001), but that the local hydration environments of the interlayer species are similar to but more ordered than those of bulk aqueous solutions (Kalinichev et al. 2000; Wang et al. 2001).

The layered structure of LDH phases allows the main-layer hydroxyl groups to donate hydrogen bonds to the interlayer anions and O atoms of the interlayer H_2O molecules (Fig. 6a). The interlayer water molecules can also form hydrogen bonds between themselves and can donate hydrogen bonds to the interlayer anions (Fig. 6b). However, in contrast to a similar
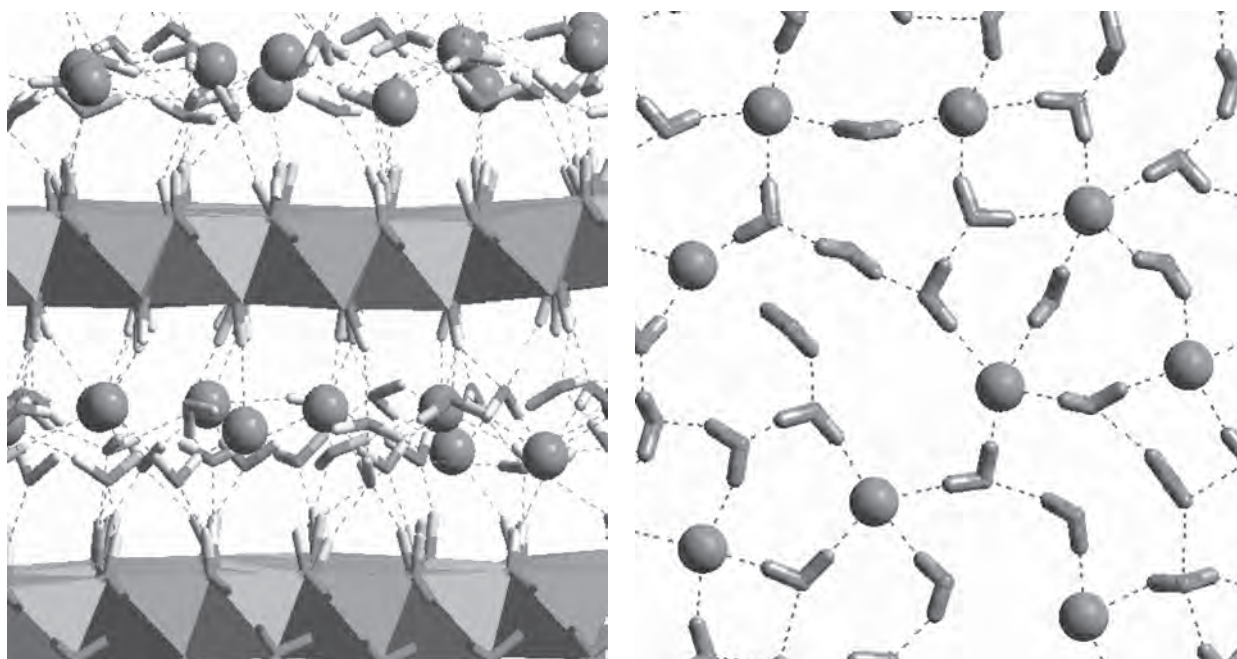
FIGURE 6. A fragment of the model Cl-bearing hydrotalcite crystal illustrating the instantaneous structure of the hydrogen-bonding network in the interlayer. (**a**) The structure viewed along the [010] direction. Balls are Cl⁻ ions and V-shaped moieties are water molecules. The dashed lines represent hydrogen bonds. The main hydroxide layer is represented by Mg/Al octahedra and OH sticks. (**b**) Interlayer Cl⁻ and H₂O molecules viewed along the [001] direction illustrating hydrogen bonding between water molecules and Cl⁻.

Li/Al-Cl LDH phase, where all anions and H$_2$O molecules are located in the middle of the interlayer and simultaneously hydrogen bond to both neighboring octahedral sheets (Hou et al. 2002), in the Mg/Al phase studied here the interlayer species are distributed between two sublayers in such a way that none of them is able to form direct hydrogen bonds to both neighboring octahedral sheets at the same time (Fig. 6a). These structural arrangements are well illustrated by the computed atom-atom radial distribution functions and the integrated atomic coordination numbers shown in Figure 7. In the interlayer of Mg/Al-Cl LDH each Cl⁻ ion on average accepts only ~2.5 hydrogen bonds from the OH groups but ~4 hydrogen bonds from the neighboring H$_2$O molecules (Fig. 7c). In contrast, in the interlayer of Li/Al-Cl LDH the situation is just the opposite, with each Cl⁻ atom accepting on average ~4 hydrogen bonds from the OH groups of the main layers interlayer and only ~2.5 hydrogen bonds from water molecules. However, the average structural environments of interlayer Cl⁻ ions the two phases are remarkably similar and also strikingly similar to the structure of the Cl⁻ hydration shell in bulk aqueous solution (thick solid lines in Figs. 7a and 7c). The average number of hydrogen bonds to the interlayer Cl⁻ ions in both LDH phases is ~6.5, and the average hydrogen bond distance is 2.21 Å, in excellent agreement with experimental data (Powell et al. 1993) and previous simulations (Smith and Dang 1994) for bulk aqueous solutions.

However, the average local structural environment of the interlayer H$_2$O molecules is quite different from that of bulk liquid water (Figs. 7b and 7d). In the Mg/Al-Cl LDH interlayer, each O atom of a water molecule accepts ~1.3 hydrogen bonds from the OH groups of the hydroxide layers and ~0.6 hydrogen bonds from other H$_2$O molecules. Thus, each of the two hydrogen atoms of any interlayer water molecule on average donates ~0.3 hydrogen bonds to neighboring H$_2$O molecules in addition to donating ~0.65 hydrogen bonds to the interlayer Cl⁻ ion (Figs. 7c and 7d). This results in a total of $\langle n_{HB}\rangle_{il} = 3.8$ as an average number of hydrogen bonds per interlayer water molecule. This coordination is significantly higher than $\langle n_{HB}\rangle_{bulk} = 3.2$ calculated for bulk liquid water (e.g., Kalinichev 2001), and closely approaches that of ice, where $\langle n_{HB}\rangle_{ice} = 4$. As we show below, these similarities and differences in the local structural environments of the interlayer species of LDHs compared to their bulk-solution behavior are also strongly correlated with the similarities and differences in their dynamic behavior reflected in the calculated diffusion coefficients and power spectra of atomic vibrations.

Importantly, the relatively weak hydrogen-bonding interactions between the interlayer species and the hydroxide sheets compared to the much stronger M-OH bonds within the hydroxide sheets lead to significant decoupling of their vibrational modes (Miyata 1983; Hernandez-Moreno et al. 1985; Cavani et al. 1991; Kagunya et al. 1997; Kagunya et al. 1998). Thus, to a good approximation, we can treat the hydroxide sheets and the interlayers as two separate substructures. Water molecules and Cl⁻ ions could each have three translational modes in the interlayer hydrogen-bonding network (Figs. 6a and 6b), but two of these modes could be degenerate due to the symmetry of the layered structure. Water molecules could also have three librational modes associated with rotational motions of H$_2$O molecules hindered by the hydrogen-bonding network.
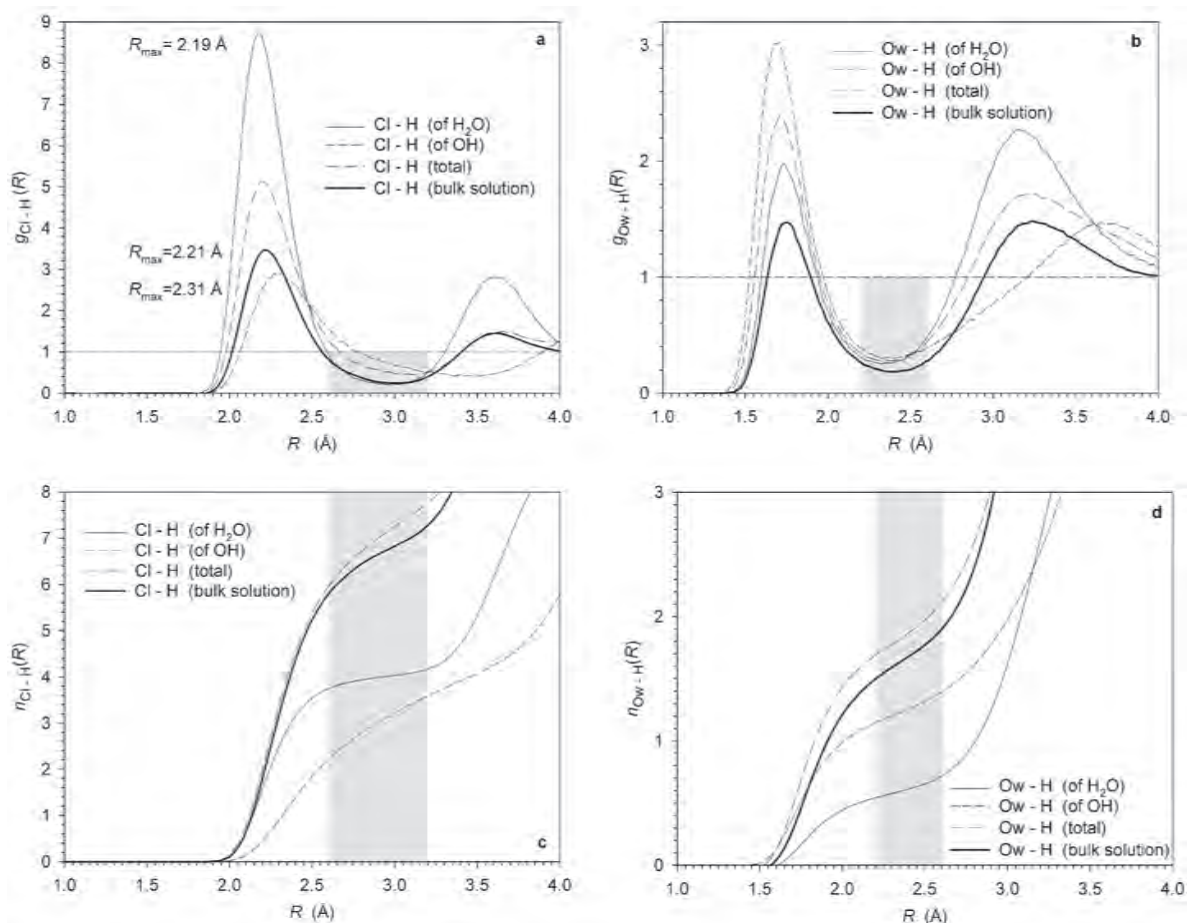
FIGURE 7. Radial distribution functions (**a**, **b**) and integrated nearest-neighbor coordination numbers (**c**, **d**) for Cl⁻-H pairs (**a**, **c**) and Ow-H pairs (**b**, **d**) in the interlayer of Mg/Al Cl-bearing hydrotalcite computed from MD simulations. Simulation results for Cl⁻ in 1.1M NaCl aqueous solution are shown as thick solid lines for comparison. Gray regions indicate the range of Cl⁻-H and Ow-H distances around the first minimum of $g(R)$ that can be reasonably used as a cutoff threshold for the formation of hydrogen bonds.

Because the molecular center of mass for H_2O nearly coincides with the center of the O atom, the translational modes of H_2O are highly correlated with the motions of the O atom, whereas the librational modes are much more pronounced in the calculated power spectra of the hydrogen atoms.

Translational modes of interlayer species

Interlayer water in our LDH model has two bands of translational modes (Fig. 3a). The band centered near 60 cm⁻¹ is associated mainly with molecular motions parallel to the layering in the **a-b** plane (XX and YY components of the VACFs), and the band centered near 210 cm⁻¹ is due mainly to ZZ motions. Interlayer Cl⁻ ions contribute to four bands (Fig. 3b). Based on analysis of their anisotropic components, the bands near 40 cm⁻¹ (mainly XX/YY motions) and near 120 cm⁻¹ (mainly ZZ motions) are comparable to those of interlayer water. The other two Cl⁻ bands involve different styles of motion. The band at 80 cm⁻¹ contains nearly equal contributions from the XX, YY, and ZZ components. Thus at this frequency, interlayer water undergoes mainly **a-b** plane translational vibrations, and the Cl⁻ vibrates equally in the **a**, **b**, and **c** directions. The Cl⁻ dy-

namics near 210 cm⁻¹ involves **a-b** translational motions parallel to the layers, whereas at this frequency interlayer water molecules move mainly in the **c** direction perpendicular to the layers.

In bulk water and ice, the two bands of translational vibrations centered near 60 and 200 cm⁻¹ are associated with the O···O···O bending and O···O stretching of hydrogen bonds respectively (e.g., Eisenberg and Kauzmann 1969). The water molecules in the first hydration shell of Cl⁻ in bulk aqueous solutions have similar modes (Bopp 1987). Due to the similarity of size and charge between Cl⁻ and O of H_2O, Cl⁻ ions can relatively easily substitute for water molecules in the hydrogen-bonding network of the interlayer. Because the interactions among Cl⁻ ions, water molecules, and OH groups of the octahedral sheet are principally due to hydrogen bonding, all translational modes are different combinations of the stretching and bending vibrations of the interlayer hydrogen-bonding network. Translations in the **a-b** plane are related mainly to the bending of hydrogen bonds between OH and the interlayer species. Translations in the **c** direction are related mainly to stretching of hydrogen bonds between OH groups and the interlayer spe-

cies. Smirnov and Bougeard (1999) have observed similar translational dynamics of interlayer H_2O molecules in their MD simulations of kaolinite.

Additionally, the zero-frequency value of the power spectrum is proportional to the self-diffusion coefficient of molecules (e.g., McQuarrie 1976). Our previous computational results for interlayer and surface H_2O molecules and Cl^- ions in LDHs show that their mobility is indeed dramatically decreased relative to that typical for bulk solutions, despite the observed similarities in their local structural and dynamic environments. This is confirmed by direct calculations of the self-diffusion coefficients (Kalinichev et al. 2000; Kalinichev and Kirkpatrick 2002). Smirnov and Bougeard (1999) found similar results in their calculations for kaolinite. On the other hand, it is worth noting that the self-diffusion coefficients calculated here for the disordered interlayer of Mg/Al-Cl LDH ($D_{Cl} = 8.2 \times 10^{-7}$ cm^2/s; $D_{H_2O} = 1.9 \times 10^{-6}$ cm^2/s) are much higher than for the more ordered interlayer of the comparable Ca$_2$Al-Cl LDH phase (Kalinichev et al. 2000; Kalinichev and Kirkpatrick 2002), for which virtually no translational mobility is observed over the 100 ps time scale of MD simulations ($D_{Cl} \approx D_{H_2O} \ll 10^{-7}$ cm^2/s). This behavior is analogous to the retarded dynamics of water molecules in the hydration shells of strongly hydrated ions such as Ca^{2+} observed in the MD simulations of bulk aqueous solutions (e.g., Bopp 1987).

Librational modes of interlayer water

The three librational modes of water molecules (hindered rotations around the molecular center of mass, schematically represented in Fig. 8a) are readily visible in the calculated power spectra of the hydrogen atoms of H_2O at 360, 430, and 540 cm^{-1} and are very useful in understanding the interlayer dynamics in LDHs. These modes can be described as twisting motion around an axis ζ corresponding to the bisector of the H-O-H angle (dipole axis), wagging motion around an axis η that is perpendicular to ζ in the plane of the molecule and parallel to the HH vector, and rocking motion around an axis ξ that is perpendicular to the plane of the molecule. Based only on the molecular moments of inertia around the different axes, the frequencies of the three librations for a free water molecule increase in the order $f_{rock} < f_{twist} < f_{wag}$ (Eisenberg and Kauzmann 1969). However, intermolecular interactions, and hydrogen bonding in particular, can affect this order (Lutz 1998). Our assignments result in the order $f_{twist} < f_{rock} < f_{wag}$, which is the same as observed in MD simulations for bulk liquid water (Lu et al. 1996). In bulk water, all three components of the simulated spectra overlap each other over a wide frequency range between 300 and 700 cm^{-1}, resulting in one broad librational band of the spectrum, in good agreement with experimentally known librational spectra of bulk water (e.g., Eisenberg and Kauzmann 1969). In contrast, in LDHs the librational bands of interlayer water are much narrower and better separated (Figs. 1a and 4a) due to the relatively greater ordering and lower mobility of water molecules in the LDH interlayers. The relatively stronger hydrogen bonds of H_2O accepted from the OH groups and the distribution of interlayer species between two sublayers keeps the H-O-H plane of the water molecules preferentially oriented at a dihedral angle of ~50 degrees with re-
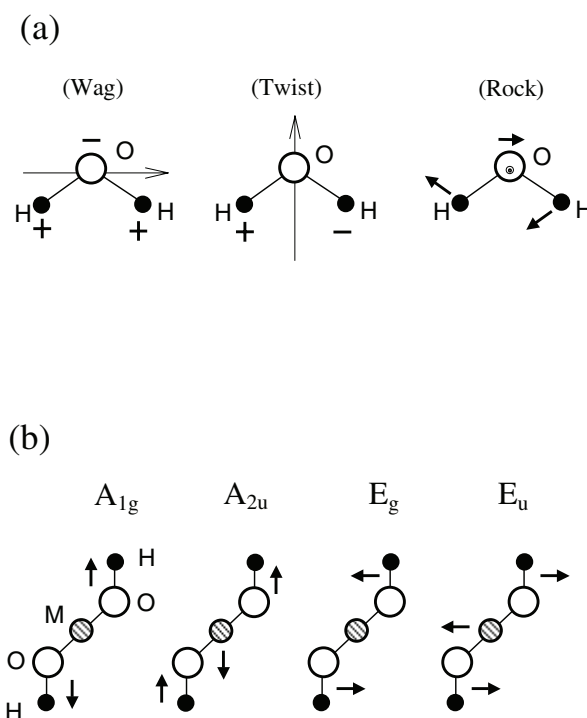

FIGURE 8. Schematic illustration of vibrational modes: (**a**) Three librational modes of an H_2O molecule. (**b**) Four lattice vibrational modes of a brucite-like octahedron.

spect to the plane of the interlayers (Figs. 6a and 6b), allowing greater rotational freedom around an axis roughly perpendicular to the layers (twisting) and the dynamical formation and breaking of hydrogen bonds to Cl^- ions and other water molecules in the interlayer (Kirkpatrick et al. 1999; Kalinichev et al. 2000; Wang et al. 2001; Hou et al. 2002).

Vibrational modes of the octahedral sheet

The principal normal modes of vibration for an ideal brucite-like structure (schematically illustrated in Fig. 8b) occur at frequencies above the FIR range studied here (Lutz et al. 1994). In LDHs, however, cation substitution and the consequent structural distortion cause some modes related to the hydroxide sheet vibrations to occur in the FIR range discussed here. Five of the most prominent modes occur at about 90, 130, 170, 250, and 290 cm^{-1} in the calculated power spectrum (Table 2), and are in good agreement with the vibrational bands observed experimentally. The principal types of motion for each of these modes can be deduced from the decomposition of the Mg, Al, and OH power spectra into XX, YY, and ZZ anisotropic components (Figs. 3, 4, and 5) and the normal mode analysis. The mode at 90 cm^{-1} involves Al and OH moving principally in the **a-b** plane with Mg moving perpendicular to this in the **c** direction. We use the notation Mg-A_{2u} + (OH,Al)-E_u to indicate this combination of motions and their relationship to the A_{2u} and E_u vibrational modes of an undistorted brucite octahedron (see Fig. 8b). The mode at 130 cm^{-1} involves vibrational motions of Mg principally in the **c** direction (Mg-A_{2u}) without significant contri-

bution from Al and OH motions. The mode at 170 cm^{-1} is mainly due to Al motions in the **c** direction, with a lesser participation of Mg and OH (Al-A_{2u} + OH-($E_u + E_g$)). Because of the higher charge and smaller atomic radius of Al, it is not surprising that the frequency of this mode is greater than for the comparable mode of Mg. A similar mode centered near 175 cm^{-1} also occurs in the recently measured FIR spectra of Al(OH)$_6$ octahedra in gibbsite and bayerite (Ruan et al. 2002).

The mode at 250 cm^{-1} involves principally Mg and Al motions in the **a-b** plane with OH also cooperatively moving parallel to this plane (Mg,Al-E_u), whereas the mode at 290 cm^{-1} involves principally OH motions in the **a-b** plane with little contribution from cation motions (OH-$E_u + E_g$). Both of these vibrational modes are also identified in the FIR spectra of hydrated alumina phases (Ruan et al. 2002). There are also two vibrational modes (330 and 480 cm^{-1}) of the octahedral sheet that are not directly visible in the full calculated or observed spectrum, because they overlap with stronger bands related to the motions of H atoms. A mode near 330 cm^{-1} involves complicated, cooperative motion of Mg, Al, and OH [Mg-($A_{2u}+E_g$) + Al-E_u], and a mode at 480 cm^{-1} is due principally to the motions of Mg in the **a-b** plane and OH motions in the **c** direction (Mg-E_u + OH-A_{1g}).

Modes related to hydrogen atoms of OH group in the octahedral sheet

The principal band involving only OH groups occurs near 370 cm^{-1} in the calculated power spectrum and involves motions of both H and O atoms in dominantly the **c** direction (OH-A_{1g}; Fig. 4b). This is the most intense band in the observed spectrum (Figs. 1a and 2a) and also dominates the FIR spectra of all aluminum hydroxide phases (Ruan et al. 2002). In the case of Mg/Al LDH, this mode overlaps with the librational modes of interlayer water molecules (Figs. 4a–b, Table 2). In addition, the modes related to H motions of OH groups in the **a-b** plane occur as a group of very broad, low intensity bands between 450 and 650 cm^{-1}. These librational motions can be visualized as complete or partial rotations of hydrogen atoms around the **c**-axis while the OH vector remains at the same angle to the **a-b** plane with no O of OH motion involved.

CONCLUDING REMARKS

Far infrared spectroscopy is one of the most useful techniques to study the structural environments and dynamics of water molecules and other ionic and molecular species confined to the interlayers or absorbed on the surface of layered minerals. It directly probes intermolecular and H-bonding interactions, but the spectra are often difficult to interpret due to the complicated pattern of atomic motions and the presence of many overlapping bands. Molecular modeling techniques, such as those used here, can be successfully applied to provide important additional information that is comparable and complementary to the measured vibrational spectra and that can significantly aid in band identification.

The principal limitation of this approach, which is also characteristic of all other semiempirical molecular modeling approaches, is the accuracy of the interatomic potentials. Here the CLAYFF force field (Cygan at al., manuscript in prepara-

tion) used in our simulations was not specifically optimized to reproduce either the structure of the vibrational properties of LDHs. Moreover, apart from the intramolecular harmonic stretching and bending terms for interlayer H$_2$O molecules and OH groups of octahedral layers, the force field model contains no explicit parameters related to the interatomic bonding and vibrations. Nevertheless, we observe a remarkably good qualitative agreement of the frequencies in the calculated power spectrum and the experimental FIR spectrum. The result clearly demonstrates that the combination of experimental vibrational spectroscopy and molecular modeling as significant potential in understanding the details of the structural and dynamic behavior of aqueous system in confined environments such as mineral interlayers, nano-pores of zeolites, biomolecular systems, and other heterogeneous fluid media dominated by hydrgen bonding.

REFERENCES CITED

Basile, F., Campanati, M., Serwicka, E., and Vaccari, A. (2001) Hydrotalcites. Introduction to the special issue. Applied Clay Science, 18, 1–2.

Bellotto, M., Rebours, B., Clause, O., Lynch, J., Bazin, D., and Elkaim, E. (1996) A reexamination of hydrotalcite crystal chemistry. Journal of Physical Chemistry, 100, 8527–8534.

Berendsen, H.J.C., Postma, J.P.M., van Gunsteren, W.F., and Hermans, J. (1981) Interaction models for water in relation to protein hydration. In B. Pullman, Ed., Intermolecular Forces, 331 p. Riedel, Dordrecht, The Netherlands.

Bopp, P. (1987) Molecular dynamics computer simulations of solvation in hydrogen bonded systems. Pure and Applied Chemistry, 59, 1071–1082.

Bougeard, D., Smirnov, K., and Geidel, E. (2000) Vibrational spectra and structure of kaolinite: A computer simulation study. Journal of Physical Chemistry B, 104, 9210–9217.

Cai, H., Hillier, A.C., Franklin, K.R., Nunn, C.C., and Ward, M.D. (1994) Nanoscale image of molecular adsorption. Science, 266, 1551–1555.

Cavani, F., Trifiro, F., and Vaccari, A. (1991) Hydratalcite-type anion clays: preparation, properties and applications. Catalysis Today, 11, 173–301.

Costantino, U., Marmottini, M., Nocchetti, M., and Vivani, R. (1998) New synthetic routes to hydrotalcite-like compounds-characterization and properties of the obtained materials. European Journal of Inorganic Chemistry, 1998, 1439–1446.

Cygan, R.T. (2001) Molecular modeling in mineralogy and geochemistry. In R.T. Cygan and J.D. Kubicki, Eds., Molecular Modeling Theory: Applications in the Geosciences, p. 1–35. Reviews in Mineralogy and Geochemistry, Mineralogical Society of America, Washington, D.C.

Dore, J. (2000) Structural studies of water in confined geometry by neutron diffraction. Chemical Physics, 258, 327–347.

Eisenberg, D. and Kauzmann, W. (1969) The Structure and Properties of Water. 296 p. Oxford University Press, Oxford.

Finch, A., Gates, P.N., Radcliffe, K., Dickson, F.N., and Bentley, F.F. (1970) Chemical Applications of Far Infrared Spectroscopy, p. 1–23. Academic Press, New York.

Frost, R.L., Ding, Z., and Kloprogge, J.T. (2000) The application of near-infrared spectroscopy to the study of brucite and hydrotalcite structure. Canadian Journal of Analytical Sciences and Spectroscopy, 45, 96–102.

Greathouse, J.A., Refson, K., and Sposito, G. (2000) Molecular dynamics simulation of water mobility in magnesium-smectite hydrates. Journal of America Chemical Society, 122, 11459–11464.

Hernandez-Moreno, M.J., Ulibarri, M.A., Rendon, J.L., and Serna, C.J. (1985) IR

characteristics of hydrotalcite-like compounds. Physics and Chemistry of Minerals, 12, 34–38.

Hill, J. and Sauer, J. (1994) Molecular mechanics potential for silica and zeolite catalysts based on ab initio calculations. 1. Dense and microporous silica. Journal of Physical Chemistry, 98, 1238–1244.

——— (1995) Molecular mechanics potential for silica and zeolite catalysts based on ab initio calculations. 2. Aluminosilicates. Journal of Physical Chemistry, 99, 9536–9550.

Hou, X. and Kirkpatrick, R.J. (2000) Solid-state ^{77}Se NMR and XRD study of the structure and dynamics of seleno-oxyanions in hydrotalcite-like compounds. Chemistry of Materials, 12, 1890–1897.

——— (2002) Interlayer structure and dynamics of ClO_4^- layered double hydroxides. Chemistry of Materials, 14, 1195–1200.

Hou, X., Kirkpatrick, R.J., Yu, P., Moore, D., and Kim, Y. (2000) ^{15}N NMR study of nitrate ion structure and dynamics in hydrotalcite-like compounds. American Mineralogist, 85, 173–180.

Hou, X., Kalinichev, A.G., and Kirkpatrick, R.J. (2002) Interlayer structure and dynamics of Cl^--$LiAl_2$ layered double hydroxide: ^{35}Cl NMR observations and molecular dynamics modeling. Chemistry of Materials, 14, 2078–2085.

Kagunya, W.W. (1996) Properties of water adsorbed in anionic clays: A neutron scattering study. Journal of Physical Chemistry, 100, 327–330.

Kagunya, W., Dutta, P.K., and Lei, Z. (1997) Dynamics of water in hydrotalcite. Physica B, 234–236, 910–913.

Kagunya W., Baddour-Hadjean, R., Kooli, F., and Jones, W. (1998) Vibrational modes in layered double hydroxides and their calcined derivatives. Chemical Physics, 236, 225–234.

Kalinichev, A.G. (2001) Molecular simulations of liquid and supercritical water: Thermodynamics, structure, and hydrogen bonding. In R.T. Cygan and J.D. Kubicki, Eds., Molecular Modeling Theory: Applications in the Geosciences, p. 83–129. Reviews in Mineralogy and Geochemistry, Mineralogical Society of America, Washington, D.C.

Kalinichev, A.G. and Kirkpatrick, R.J. (2002) Molecular dynamics modeling of chloride binding to the surfaces of Ca hydroxide, hydrated Ca-aluminate and Ca-silicate phases. Chemistry of Materials, 14, 3539–3549.

Kalinichev, A.G., Kirkpatrick, R.J., and Cygan, R. T. (2000) Molecular modeling of the structure and dynamics of the interlayer and surface species of mixed-metal layered hydroxides: chloride and water in hydrocalumite (Friedel's salt). American Mineralogist, 85, 1046–1052.

Kirkpatrick, R.J., Yu, P., Hou, X., and Kim, Y. (1999) Interlayer structure, anion dynamics, and phase transitions in mixed-metal layered hydroxides: variable temperature ^{35}Cl NMR spectroscopy of hydrotalcite and Ca-aluminate hydrate. American Mineralogist, 84, 1186–1190.

Kleinhesselink, D. and Wolfsberg, M. (1992) The evaluation of power spectra in molecular dynamics simulations of anharmonic solids and surface. Surface Science, 262, 189–207.

Kloprogge, J.T., Hickey, L., and Frost, R.L. (2001) Heating stage Raman and infrared emission spectroscopic study of the dehydroxylation of synthetic Mg-hydrotalcite. Applied Clay Science, 18, 37–49.

Kubicki, J.D. (2001) Interpretation of vibrational spectra using molecular orbital theory calculations. In R.T. Cygan and J.D. Kubicki, Eds., Molecular Modeling Theory: Applications in the Geosciences, p. 459–483. Reviews in Mineralogy and Geochemistry, Mineralogical Society of America, Washington, D.C.

Lu, T., Toth, G., and Heinzinger, K. (1996) Systematic study of the spectroscopic properties of isotopically substituted water by MD simulations. Journal of Physical Chemistry, 100, 1336–1339.

Lutz, H.D. (1998) Bonding and structure of water molecules in solid hydrates. Correlation of spectroscopic and structure data. Structure and Bonding, 69, 97–125.

Lutz, H.D., Moller, H., and Schmidt, M. (1994) Lattice vibration spectra. Part LXXXII. Brucite-type hydroxides $M(OH)_2$ (M = Ca, Mn, Co, Fe, Cd)—IR and Raman spectra, neutron diffraction of $Fe(OH)_2$. Journal of Molecular Structure, 328, 121–132.

McMillan, P.F. and Hess, A.C. (1988) Symmetry, group theory and quantum mechanics. In F.C. Hawthorne, Ed., Spectroscopic Methods in Mineralogy and Geology, p. 11–61. Reviews in Mineralogy, Mineralogical Society of America, Washington, D.C.

McQuarrie, D.A. (1976) Statistical mechanics, 641 p. Harper & Row Publishers, New York.

Miyata, S. (1975) The synthesis of hydrotalcite-like compounds and their structures and physical-chemical properties—I: The systems Mg^{2+}-Al^{3+}-NO_3^-, Mg^{2+}-Al^{3+}-Cl^-, Mg^{2+}-Al^{3+}-ClO_4^-, and Ni^{2+}-Al^{3+}-Cl^- and Zn^{2+}-Al^{3+}-Cl^-. Clays and Clay Minerals, 23, 369–375.

——— (1983) Anion-exchange properties of hydrotalcite-like compounds. Clays and Clay Minerals, 31, 305–311.

Molecular Simulations Inc. (1999) Cerius2-4.0 User Guide. Forcefield-Based Simulations; MSI, San Diego.

Nandi, N., Bhattacharyya, K., and Bagchi, B. (2000) Dielectric relaxation and solvation dynamics of water in complex chemical and biological systems. Chemical Reviews, 100, 2013–2045.

Newman, S. and Jones, W. (1998) Synthesis, characterization and applications of layered double hydroxides containing organic guests. New Journal of Chemistry, 22, 105–115.

Powell, D.H., Neilson, G.W., and Enderby, J.E. (1993) The structure of Cl^- in aqueous-solution—an experimental determination of $G_{Cl-H}(R)$ and $G_{Cl-O}(R)$. Journal of Physics—Condensed Matter, 5, 5723–5730.

Ruan, H.D, Frost, R.L., Kloprogge, J.T., and Duong, L. (2002) Far-infrared spectroscopy of alumina phases. Spectrochimica Acta Part A, 58, 265–272.

Smirnov, K.S. and Bougeard, D. (1999) A molecular dynamics study of structure and short-time dynamics of water in kaolinite. Journal of Physical Chemistry B, 103, 5266–5273.

Smith, D.E. and Dang, L.X. (1994) Computer simulations of NaCl association in polarizable water. Journal of Chemical Physics, 100, 3757–3766.

Swenson, J., Bergman, R., and Howells, W.S. (2000) Quasielastic neutron scattering of two-dimensional water in a vermiculite clay. Journal of Chemical Physics, 113, 2873–2879.

Taylor, H. (1973) Crystal structure of some double hydroxide minerals. Mineralogical Magazine, 39, 377–389.

Teleman, O., Jönsson, B., and Engström, S. (1987) A molecular dynamics simulation of a water model with intramolecular degrees of freedom. Molecular Physics, 60, 193–203.

Teppen, B.J., Rasmussen, K., Bertsch, P.M., Miller, D.M., and Schafer, L. (1997) Molecular dynamics modeling of clay minerals. 1. Gibbsite, kaolinite, pyrophyllite, and beidellite. Journal of Physical Chemistry B, 101, 1579–1587.

Terzis, A., Filippakis, S., Kuzel, H.-J., and Burzlaff, H. (1987) The crystal structure of $Ca2Al(OH)6Cl·2H2O$. Zeitschrift für Kristallographie, 181, 29–34.

Vucelic, M., Jones, W., and Moggridge, G.D. (1997) Cation ordering in synthetic layered double hydroxides. Clays and Clay Minerals, 45, 803–817.

Yao, K., Taniguchi, M., Nakata, M., Takahashi, M., and Yamagishi, A. (1998) Nanoscale image of molecular adsorption of metal complexes on the surface of a hydrotalcite crystal. Langmuir, 14, 2410–2414.

Wang, J., Kalinichev, A.G., Kirkpatrick, R.J., and Hou, X. (2001) Molecular modeling of the structure and energetics of hydrotalcite hydration. Chemistry of Materials, 13, 145–150.